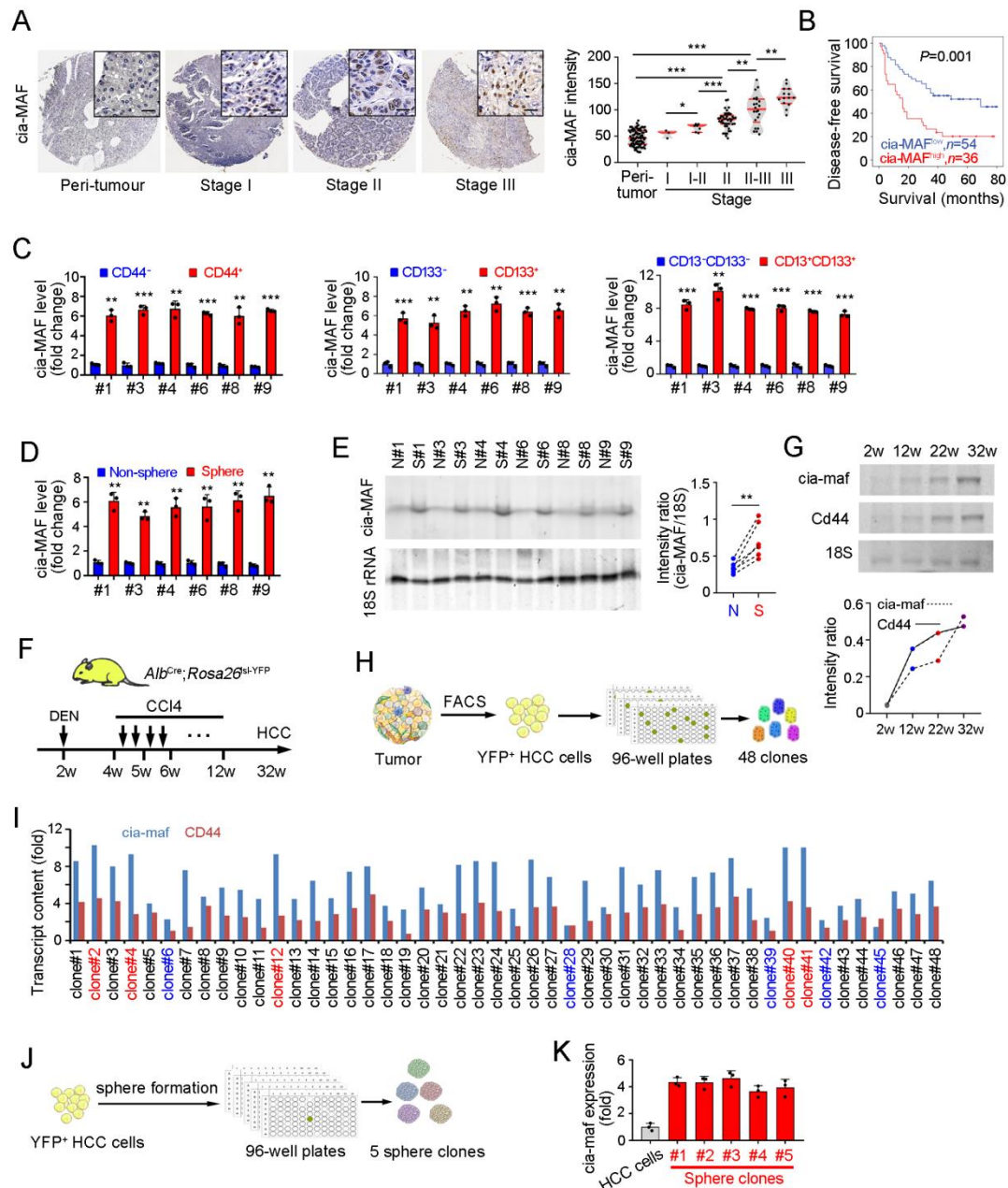
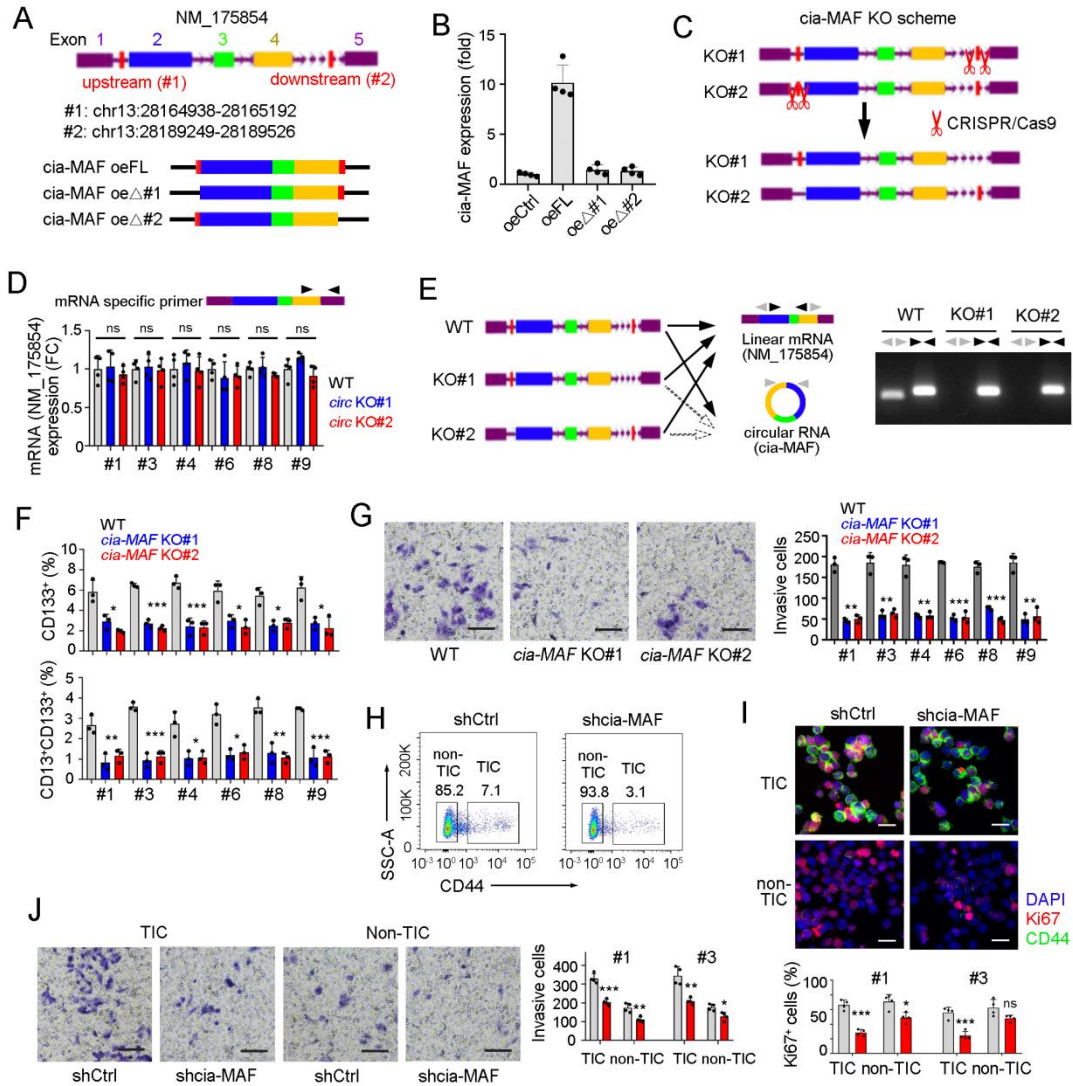


Supplemental Figure 1. Characteristics of circRNA expression in liver TICs. (A) Real-time PCR analysis for circRNA in CD44⁺ TICs and CD44⁻ non-TICs, which were sorted from primary HCC sample #1. Top 10 circRNAs highly expressed in TICs were labeled blue. (B) Real-time PCR to detect circRNA levels after RNase R (upper) or actinomycin D (lower) treatment. For upper panel, total RNA was treated with RNase R (3U RNase R per μg RNA) for 1 hour. For lower panel, TICs were treated with 2 $\mu\text{g}/\text{ml}$ actinomycin D (Act-D) for 2 hours. (C) Real-time PCR detection for knockdown efficiency of the indicated circRNAs in TICs. (D) Sphere formation assay of primary cells in which the indicated circRNA was silenced individually. Sphere formation ratios in the left panel and typical images in the right panel. * $P < 0.05$, by 1- way ANOVA. Scale bars, 500 μm . For all panels, $n=3$ independent experiments, and data are shown as mean \pm s.d.



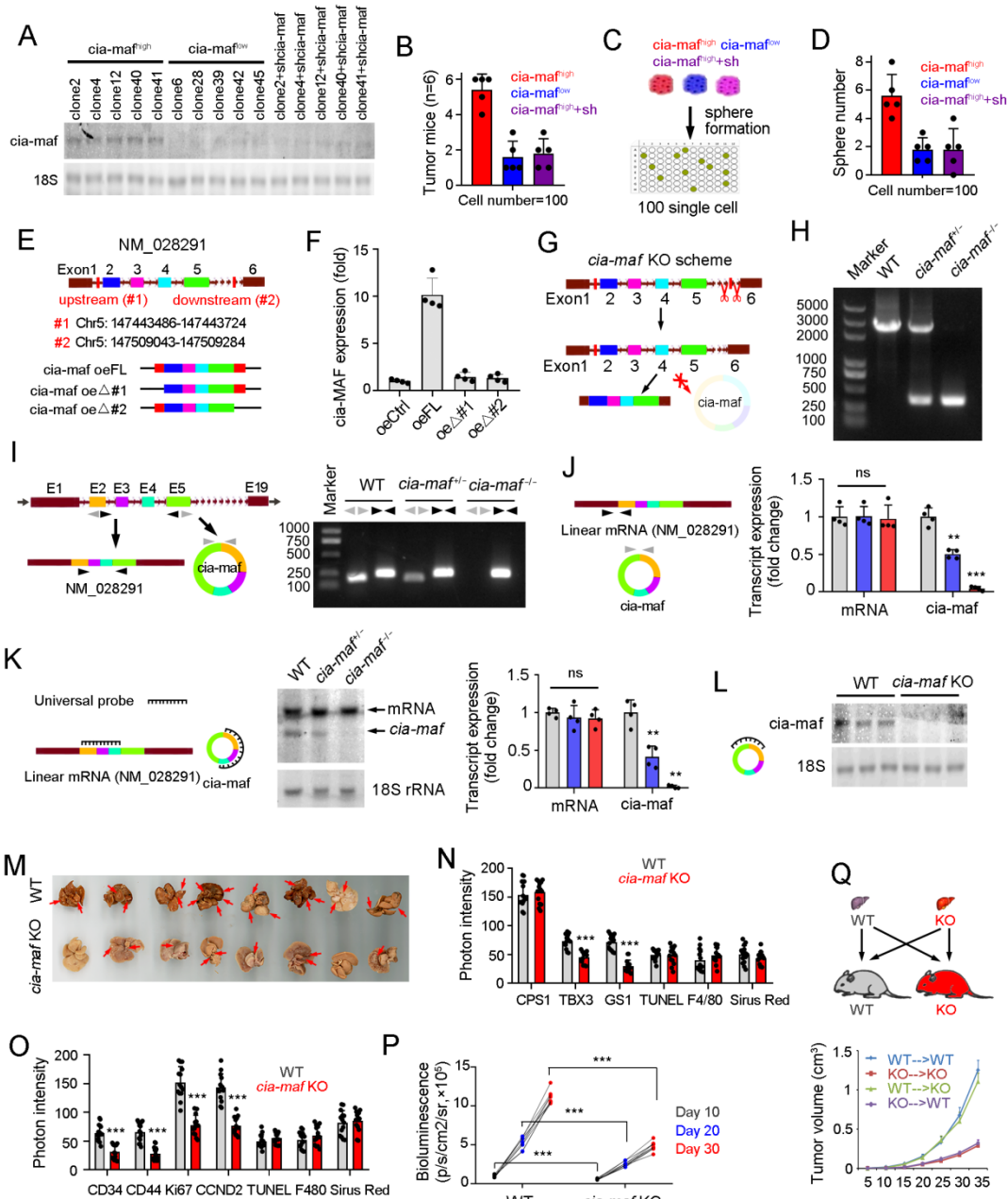
Supplemental Figure 2. cia-MAF is highly expressed in liver TICs. (A) In situ hybridization of cia-MAF in HCC tissue microarray. Typical images were in the left panels and calculated intensities were in the right panel. Scale bars, 30 μ m. The details of HCC tissue microarray were listed in Supplemental Table 5. (B) Kaplan–Meier survival analysis of cia-MAF high-expressed and low-expressed samples, which were grouped according to the average cia-MAF expression level. (C, D) Real-time PCR for cia-MAF expression in TICs and non-TICs (C), or spheres and non-spheres (D). cia-MAF expression levels were normalized to those in non-TIC cells (C) or non-spheres (D). In C, CD44⁺, CD133⁺ and CD13⁺CD133⁺ TICs were enriched for cia-MAF detection. (E) Northern blot of cia-MAF in spheres (S) and non-spheres (N). 18 rRNA is a loading control. (F) Schematic diagram of mouse DEN/CC14 liver tumorigenesis. 2-week old *Alb^{Cre}; Rosa26^{Isl-YFP}* mice were used for DEN treatment. (G) Northern blot for cia-maf expression in YFP⁺ cells of

Alb^{Cre}; *Rosa26*^{Isl-YFP} mice, which were treated with DEN/CCI4 for the indicated time points. (H) Schematic diagram of monoclonalization of DEN/CCI4 tumors. (I) *cia-maf* and CD44 expression levels in the individual clones. 48 clones were detected, and the top 5 *cia-maf*^{high} and *cia-maf*^{low} clones were labeled as red and blue, respectively. (J) Schematic diagram of sphere formation derived from single cells. (K) *cia-MAF* expression levels of five sphere clones, and all expression levels were normalized to those in HCC cells. In all panels, data are shown as mean \pm s.d. **P* < 0.05; ***P* < 0.01; ****P* < 0.001. Significance was determined by 1-way ANOVA (A), log-rank test (B) or one-tailed Student's *t* test (C-E). All data represent *n*=3 independent experiments.



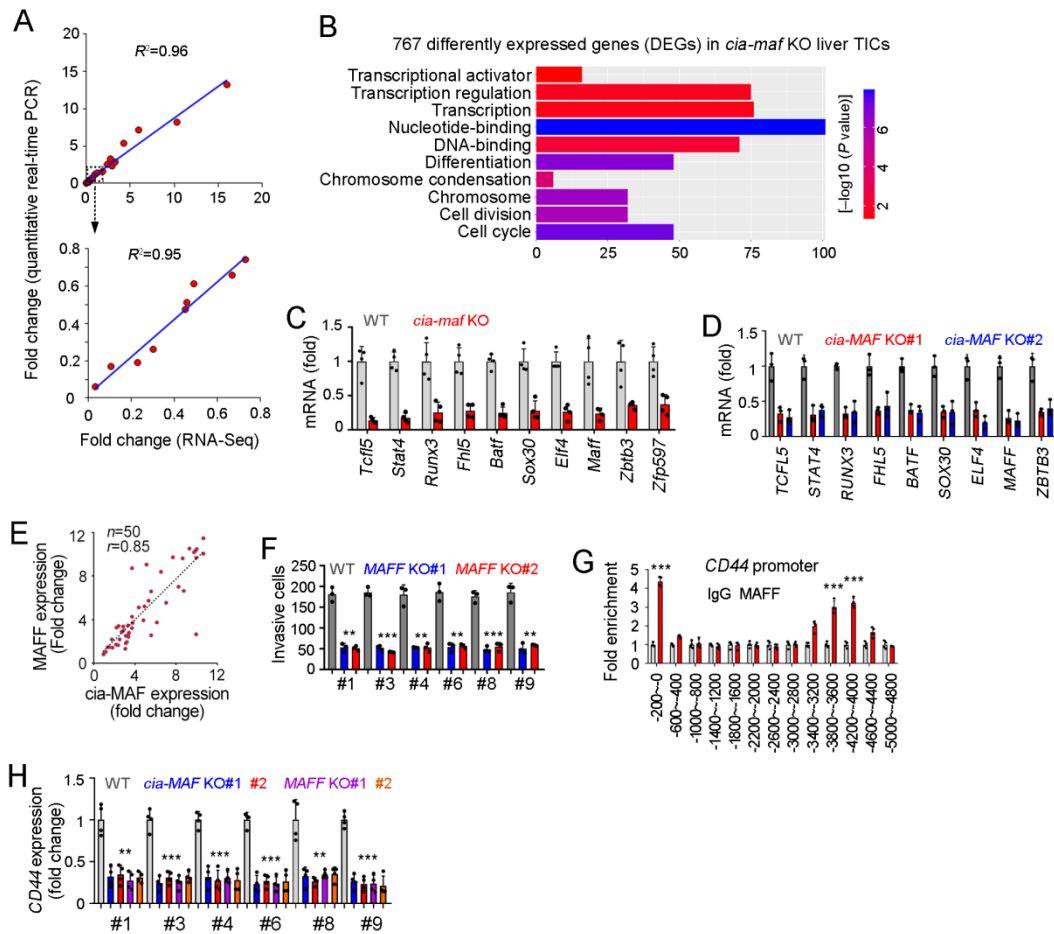
Supplemental Figure 3. Impaired self-renewal in *cia-MAF* knockout cells. (A, B) Minigene assay for the necessity of upstream and downstream reverse complementary sequences in *cia-MAF* biogenesis. FL, full length, Δ 1, full length without upstream sequence, Δ 2, full length without downstream sequence. (C) Schematic diagram of CRISPR/Cas9 based *cia-MAF* knockout strategy. Upstream and downstream reverse complementary sequences were deleted in KO#1 and KO#2 cells, respectively. (D) Realtime PCR to detect the expression levels of *cia-MAF* linear gene (NM_175854) in *cia-MAF* knockout (*circ* KO) cells and WT cells. Six primary samples were used and all expression levels were normalized to those in WT cells. (E) WT, *cia-MAF* KO#1 and *cia-MAF* KO#2 cells were obtained to detect the expression levels of linear mRNA and circular RNA by PCR. Black arrowheads denote primers for linear mRNA (NM_175854) detection, and gray arrowheads denote primers for circular RNA (*cia-MAF*) detection. Impaired *cia-MAF* expression and comparable linear mRNA expression were detected in *cia-MAF* knockout cells. (F) FACS detection of CD133⁺ TICs (upper) or CD13⁺CD133⁺ TICs (lower) in *cia-MAF* knockout and WT cells. (G) Tumor invasion capacity of *cia-MAF* knockout and control cells, with representative images in the left panel and calculated data in the right panel. Scale bars, 100 μ m. (H-J) *cia-MAF* silenced and control primary

HCC#1 cells were established via lentivirus, and CD44⁺ TICs and CD44⁻ non-TICs were sorted with FACS (H), followed by Ki67 staining (I) and transwell assay (J). Scale bars, I, 20 μm ; J, 100 μm . In all panels, data are shown as mean \pm s.d. * $P < 0.05$; ** $P < 0.01$; *** $P < 0.001$. Significance was determined by 1-way ANOVA (D, F, G) or one-tailed Student's t test (I, J). For G, $n=3$ independent experiments; for H-J, $n=4$ independent experiments were performed with similar results.

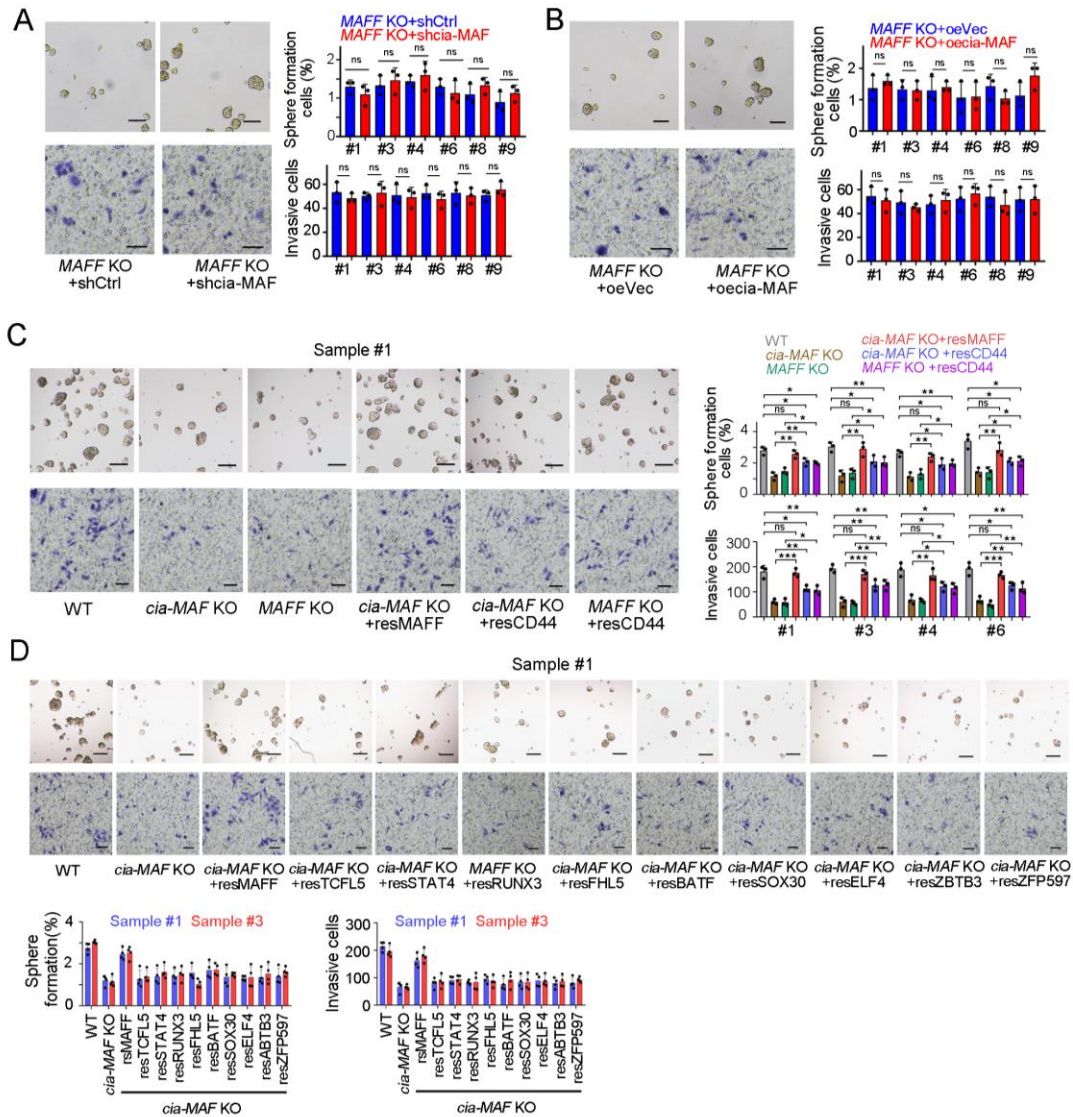


Supplemental Figure 4. Generation of *cia-maf* knockout mice. (A) Northern blot to confirm *cia*-MAF knockdown efficiency in *cia*-MAF^{high} clones. (B) Tumor formation capacity of *cia*-MAF^{high} clones, *cia*-MAF^{low} clones and *cia*-MAF silenced *cia*-MAF^{high} clones. Five clones were used for each group, 100 cells per clone and $n=6$ mice used for tumor initiation. (C, D) Sphere formation of *cia*-MAF^{high} clones, *cia*-MAF^{low} clones and *cia*-MAF silenced *cia*-MAF^{high} clones. $n=5$ clones and 100 single cells were used per clone. (E, F) Minigene assay for the necessity of upstream and downstream reverse complementary sequences in *cia-maf* biogenesis. FL, full length, $\Delta 1$, full length without upstream sequence, $\Delta 2$, full length without downstream sequence. (G) Schematic diagram of CRISPR/Cas9 based *cia-maf* knockout strategy. The downstream reverse complementary sequence was deleted via CRISPR/Cas9 approach. (H) WT, *cia-maf*^{+/-} and *cia-maf*^{-/-} livers were identified by agarose gel electrophoresis. WT allele had PCR

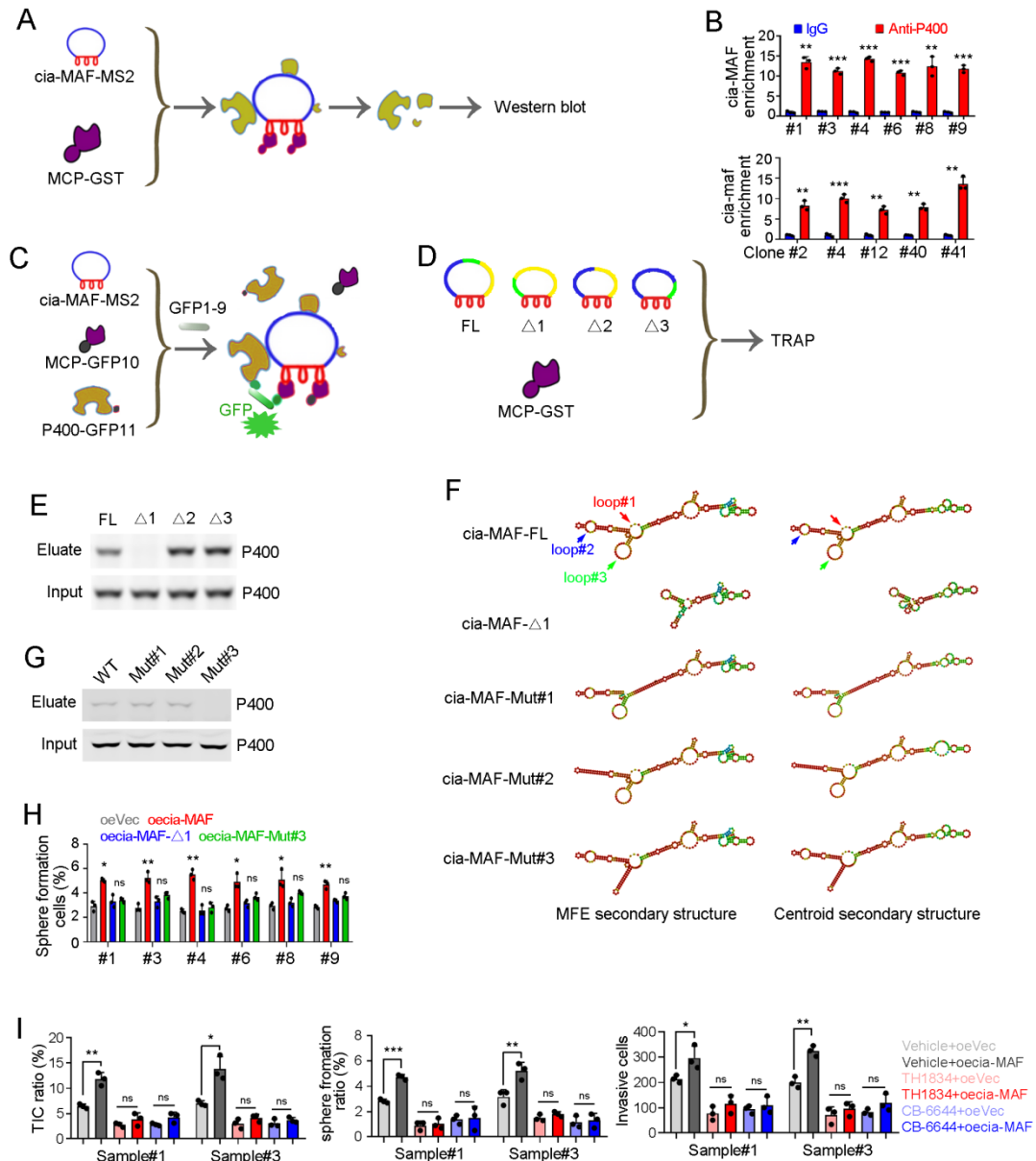
products of 2727 bp in length and deficient allele had PCR products of 343 bp in length. (I) WT, *cia-maf*^{+/-} and *cia-maf*^{-/-} livers were obtained to confirm *cia-maf* knockout by PCR. Black arrowheads denote primers for linear mRNA detection, and the sequences are: 5'-CCAGCTTTATTGGAGTCAAT-3' and 5'-AGGTTGATCCTCCTTTAGGT-3'. Gray arrowheads denote primers for circular RNA (*cia-maf*) detection, and the sequences are: 5'-ACCTAAAGGAGGATCAACCT-3' and 5'-ATTGACTCCAATAAAGCTGG-3'. The length of linear mRNA and circular RNA PCR product was 249 bp and 199 bp. (J) Linear mRNA and circular RNA were detected through quantitative real-time PCR with specific primers. Black arrowheads are linear mRNA primers: 5'-CTACTACGCCAAGGACAAGA-3' and 5'-ATTGACTCCAATAAAGCTGG-3', Gray arrowheads are circular RNA primers: 5'-ACCTAAAGGAGGATCAACCT-3' and 5'-ATTGACTCCAATAAAGCTGG-3'. (K) Northern blot to detect the linear and circular RNA simultaneously with a universal probe, which cover the first 3 exons and obtained through in vitro transcription. Typical images and calculated results from $n = 4$ independent experiments were shown. (L) Northern blot for *cia-maf* knockout efficiency, with 18S rRNA as a loading control. *cia-maf* probe was designed to target the conjunction sequence of *cia-maf*. (M) Tumor images of DEN/CCI4 induced liver tumorigenesis in WT and *cia-maf* KO mice. Tumors were denoted by red arrows. (N, O) Photon intensities were measured in the indicated staining pictures, for which peri-tumor liver tissues (N) and tumors (O) from WT and *cia-maf* KO mice were used. For each mice, $n=10$ fields were measured and the average intensities were calculated. (P) Average bioluminescence signals at the indicated times after hydrodynamic expression of HrasG12V/shP53 and luciferase/SB transposases. $n=10$ mice were used for each panel. (Q) Liver tumor transplantation assays to detect cell-intrinsic or cell-extrinsic role of *cia-maf*. 1×10^6 CCI4/DEN induced *cia-maf* KO or control liver tumor cells were subcutaneously injected into *cia-maf* KO or control mice, and tumor volumes were measured in the indicated time points. Schematic diagram of liver tumor transplantation assays was in the upper panel, and tumor volume curve was shown in the lower panel. For H-Q, WT littermates were used as controls. In all panels, data are shown as mean \pm s.d. ** $P < 0.01$, *** $P < 0.001$, ns, not significant. Significance was determined by 1-way ANOVA (J, K) or one-tailed Student's t test (N-P). For E-L, $n=4$ independent experiments were performed with similar results.



Supplemental Figure 5. *cia*-MAF targeted MAFF. (A) Confirmation of RNA sequencing data with real-time PCR. $n=20$ genes are randomly selected and examined, RNA sequencing results and real-time PCR results were shown in horizontal and vertical axis, respectively. (B) WT and *cia-MAF* KO TICs were used for RNA sequencing, followed by gene ontology analysis. Transcription-associated genes are enriched. (C) Real-time PCR to detect the expression levels of indicated TFs in WT and *cia-MAF* KO liver cancer cells. All expression levels were normalized to those in WT cells. (D) Real-time PCR for TF detection in *cia-MAF* knockout and control cells. (E) Co-expression of *cia*-MAF and MAFF expression in 50 primary tumor samples. All expression levels were normalized to the average levels of peri-tumor samples. (F) Transwell assay was performed using MAFF knockout primary cells, and the numbers of invasive cells were shown. (G) Quantitative real-time PCR to detect the enrichment of *CD44* promoter in ChIP eluate, in which sphere lysate from primary #1, MAFF antibody and control antibody were used. (H) Quantitative real-time PCR for *CD44* expression in *cia*-MAF KO, MAFF KO and WT cells. All expression levels were normalized to those in WT cells. In all panels, data are shown as mean \pm s.d. ** $P < 0.01$, *** $P < 0.001$, by 1-way ANOVA (F, H) or one-tailed Student's t test (G). For D, F, $n=3$ independent experiments; for C, G, H, $n=4$ independent experiments.

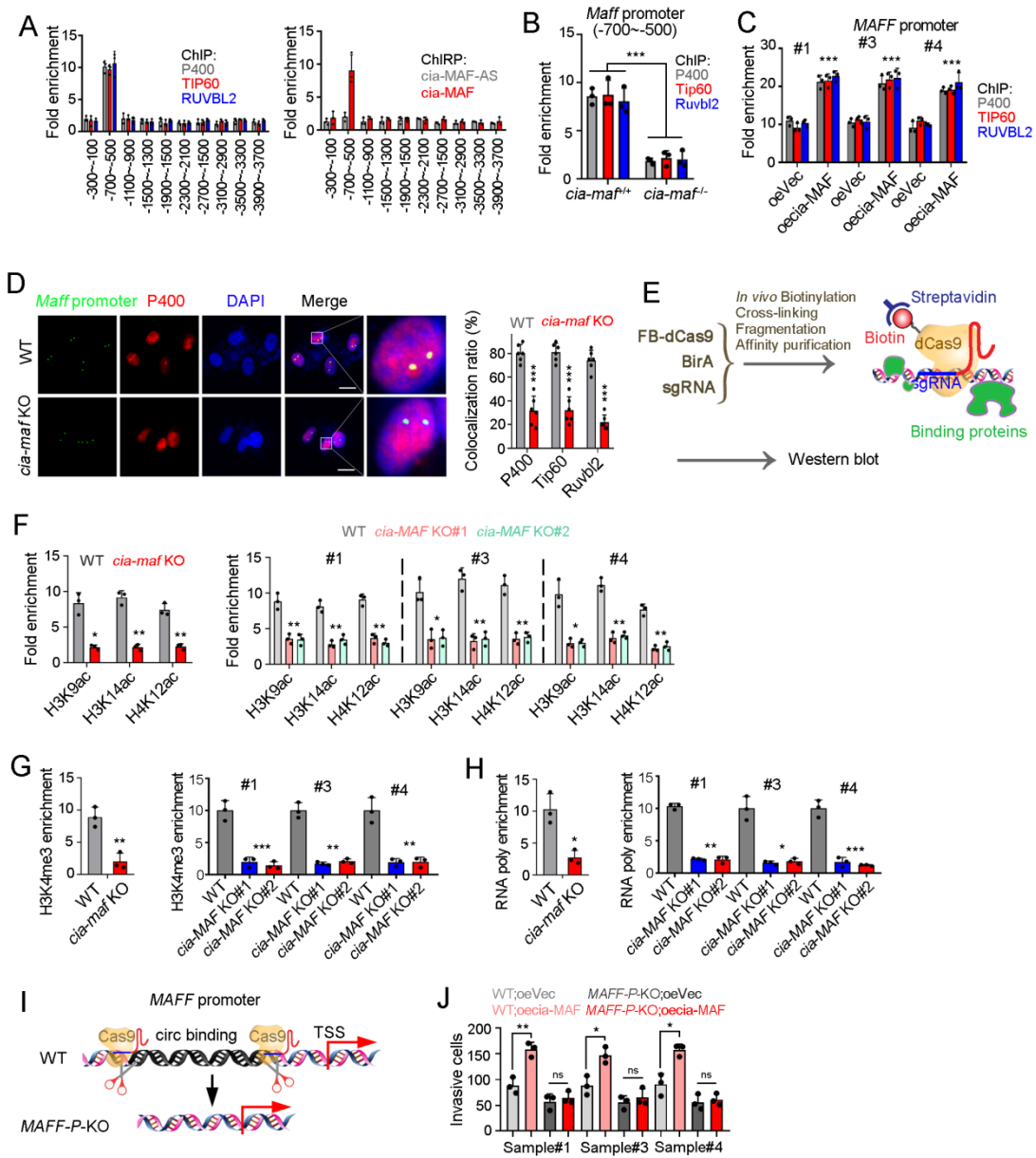


Supplemental Figure 6. *cia*-MAF exerted its role mainly through MAFF. (A) Sphere formation (upper) and transwell assay (lower) of *cia*-MAF silenced cells, which were established in *MAFF* knockout cells. (B) *cia*-MAF overexpression in *MAFF* knockout cells, followed by sphere formation assay (upper) and transwell assay (lower). (C) Sphere formation (upper) and transwell (lower) assays using *cia*-MAF knockout, *MAFF* knockout, *MAFF* rescued and CD44 rescued cells. Typical images were shown in the left panels and calculated ratios were shown in the right panels. (D) The indicated TFs were rescued in *cia*-MAF knockout cells, followed by sphere formation (upper) and transwell (lower) detection. In all panels, data are shown as mean \pm s.d. * $P < 0.05$, ** $P < 0.01$, *** $P < 0.001$; ns, not significant, by one-tailed Student's t-test (A, B, D) or 1-way ANOVA (C). $n=3$ (A-C) or $n=4$ (D) independent experiments were performed with similar results.



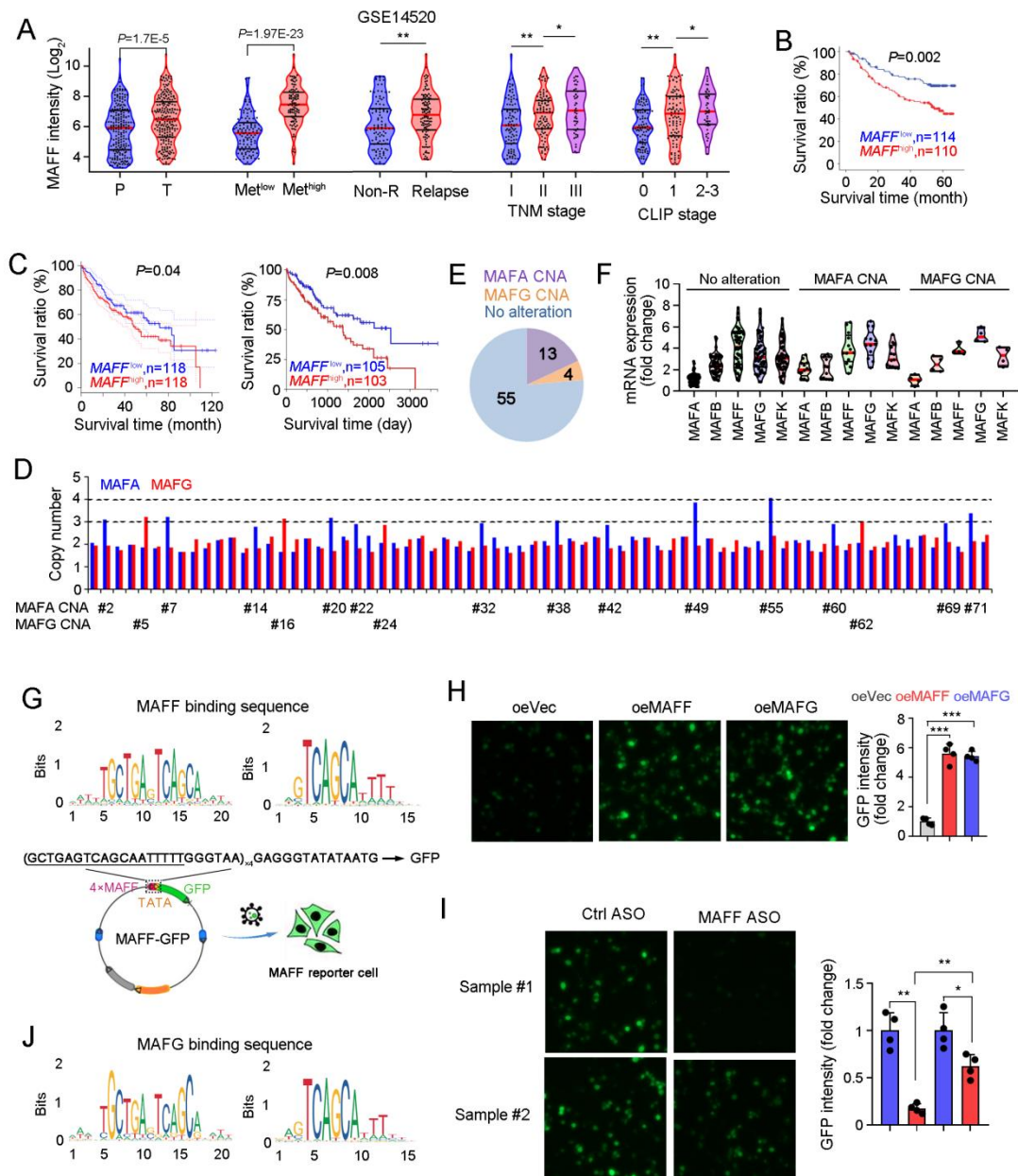
Supplemental Figure 7. cia-MAF interacts with TIP60 complex. (A) Schematic diagram of TRAP assay. MS2 conjugated cia-MAF and MCP-GST were used for cia-MAF pulldown, followed by Western blot analysis for binding proteins. (B) Real-time PCR of cia-MAF enrichment in RNA immunoprecipitation (IP) eluate using P400 antibody and human (upper) or mouse (lower) spheres. $n=3$ independent experiments. (C) Schematic diagram of GFP split assay. cia-MAF-MS2, MCP-GFP10, P400-GFP11 and GFP1-9 were used for GFP split assay. (D) TRAP assay with indicated truncate cia-MAF. FL, full length; $\Delta 1$, deleting #1 exon; $\Delta 2$, deleting #2 exon; $\Delta 3$, deleting #3 exon. (E) Western blot of P400 in eluate from TRAP assay using sphere lysate and indicated truncate cia-MAF. (F) Prediction of stem-loop structures of cia-MAF and mutant cia-MAF. Predictions were based on minimum free energy (MFE, left) and Centroid secondary structure (right). Color scales denote confidence of predictions for each base with shades of red indicating strong confidence (<http://rna.tbi.univie.ac.at/>). (G) Western blot of P400 in eluate from TRAP

assay using the sphere lysate and indicated mutant cia-MAF. (H) Sphere formation assay using liver cancer cells, in which cia-MAF, truncate cia-MAF or mutant cia-MAF were overexpressed. (I) TIC FACS detection, sphere formation assay and transwell assay of cia-MAF overexpressing cells treated with TIP60 inhibitors. In all panels, data are shown as mean \pm s.d. * P < 0.05; ** P < 0.01; *** P < 0.001; ns, not significant, by one-tailed Student's t-test. All data represent $n=3$ independent experiments.



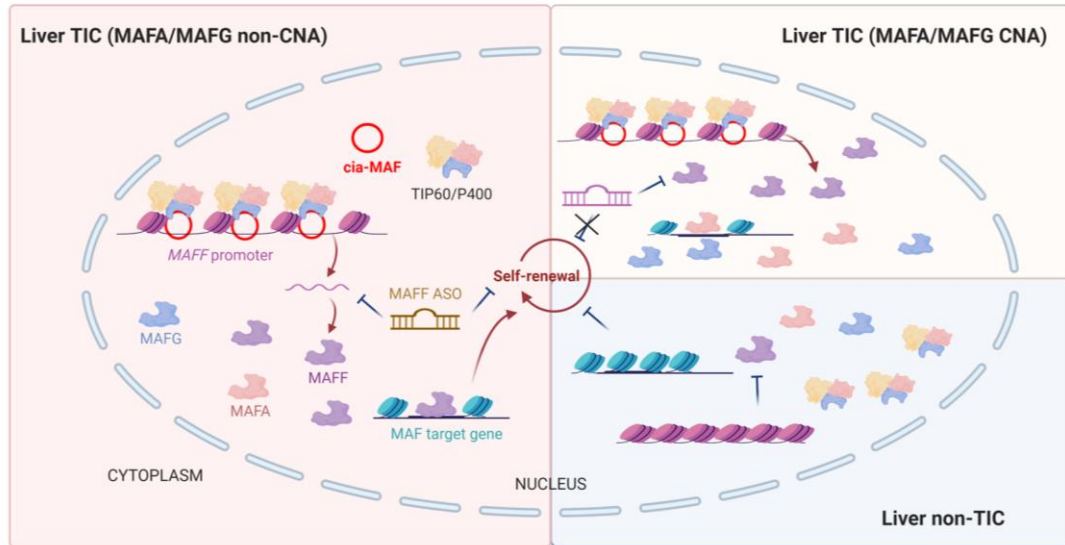
Supplemental Figure 8. *cia*-MAF recruits TIP60 complex to *MAFF* promoter. (A) Real-time PCR for *MAFF* promoter enrichment in elute of ChIP and ChIRP assay using spheres. (B) Real-time PCR to detect the enrichment of *Maff* promoter in eluate from ChIP assay using TIP60 antibody and *cia*-*Maf* knockout spheres. (C) Real-time PCR for *MAFF* promoter enrichment in ChIP eluate, for which *cia*-MAF overexpressing and control spheres were used. (D) Double fluorescence in situ hybridization assay for the co-localization of *Maff* promoter and P400 in WT and *cia-maf* KO liver cancer cells. Typical images were shown in the left panel and co-localization ratios in the right panel. (E) Schematic diagram of CRISPR affinity purification in situ of regulatory elements (CAPTURE) assay, which was used to analyze the binding proteins of a specific DNA region. (F) Real-time PCR of *MAFF* promoter in H3K9ac, H3K14ac and H4K12ac ChIP eluate, in which WT and *cia-maf* KO mice (left), or *cia*-MAF knockout and control cells (right) were used. IgG was used as control. (G) Real-time PCR of *MAFF* promoter in

H3K4me3 ChIP eluate, using WT and *cia-maf* KO cells (left), or *cia-MAF* knockout and control cells (right). (H) Real-time PCR of *MAFF* promoter in RNA Polymerase II (RNA poly) ChIP eluate, using WT and *cia-maf*KO cells (left), or *cia-MAF* knockout and control cells (right). (I) Schematic diagram of generating *MAFF* promoter knockout (*MAFF-P-KO*) cells. A pair of sgRNA was used to delete *cia-MAF* binding sequence of *MAFF* promoter. (J) Tumor invasion capacity upon *cia-MAF* overexpression, which were generated in WT and *MAFF-P-KO* cells. For F-H, WT littermates were used as controls. * $P < 0.05$; ** $P < 0.01$; *** $P < 0.001$; ns, not significant, by 1-way ANOVA (B, C, F-H) or one-tailed Student's t-test (D, J). For A-C, F-H, J, $n=3$ independent experiments; for D, $n=6$ mice per group, and 100 cells were observed for each mice.



Supplemental Figure 9. MAFF serves as a target of liver TICs. (A) Violin plot plots for MAFF expression in tumor (T), peri-tumor (P), high-metastasis (Met^{high}), low-metastasis (Met^{low}), Relapse, non-relapse (non-R) and HCC samples with different clinical stages. TNM: tumour node metastasis; CLIP: cancer of the liver Italian program. Online-available dataset GSE14520 (<https://www.ncbi.nlm.nih.gov/geo/query/acc.cgi?acc=GSE14520>) were used for MAFF expression analysis, and patient details were listed in Supplemented Table 6. (B) Kaplan–Meier survival analysis of MAFF^{high} and MAFF^{low} samples. HCC samples were divided into two groups according to MAFF expression levels. (C) MAFF survival analyses were performed by GEPIA (<http://gepia2.cancer-pku.cn/#survival>, left) or TCGA (<https://xenabrowser.net/>, right). (D, E) Real-time PCR for MAFA/MAFG copy number detection in the indicated HCC samples. For D, MAFA and MAFG CNA samples were listed below. CNA, copy number alteration. All number details were shown in D and pie chart shown in E. (F) Violin plot showing the expression levels of MAF (including

MAFA, MAFB, MAFF, MAFG and MAFK) in HCC samples with no MAFA/MAFG CNA, MAFA CNA, and MAFG CNA. Individual samples are shown with medium levels (red), minimum, maximum and quarter levels. (G) MAFF reporter plasmid was constructed and MAFF-reporter 293T cells were generated. MAFF binding motifs were obtained from Jaspar (<http://jaspar.genereg.net/>). (H) The response of MAFF-reporter 293T cells to MAFF and MAFG overexpression was observed through fluorescence microscope. Typical images were shown in the left panel and calculated results were in the right panel. oe, overexpression. (I) MAFF-reporter primary cells were generated and treated with 50nM MAFF ASO or control ASO, and the GFP signaling in CD44⁺ TICs were observed. Typical images were shown in the left panel and calculated results were in the right panel. (J) MAFG binding motifs were obtained from Jaspar (<http://jaspar.genereg.net/>). In all panels, data are shown as mean \pm s.d. * $P < 0.05$; ** $P < 0.01$; *** $P < 0.001$, by one-tailed Student's t-test (A, H, I) or log-rank test (B, C). All data represent $n=4$ independent experiments.



Supplemental Figure 10. Work model of cia-MAF in liver TICs. Circular RNA cia-MAF is highly-expressed in liver TICs and drives the expression of MAFF via recruiting TIP60/P400 complex to *MAFF* promoter. MAFF is a potential target for liver TIC elimination, especially in HCC samples without MAFA/MAFG copy number alternation.